Proceedings of the Thirty-third (2023) International Ocean and Polar Engineering Conference **www.isope.org**
Ottawa, Canada, June 19-23, 2023

ISBN 978-1-880653-80-7; ISSN 1098-6189

High-fidelity Modeling and Simulation Approach for Bow Wave Breaking of a KRISO Container Ship

*Yuming Shao[1], Wentao Wang[1,2], Jianhua Wang[1], Decheng Wan[1]**

[1]Computational Marine Hydrodynamics Lab (CMHL), School of Naval Architecture, Ocean and Civil Engineering, Shanghai Jiao Tong University, Shanghai, China
[2] China Ship Scientific Research Center, Wuxi, China
*Corresponding author

ABSTRACT

Bow wave breaking is very obvious for ship advancing in open sea, where strong nonlinear phenomenon, such as violent free surface and air-entrainment, can be observed. It is quite challenging to accurate predict the ship bow wave breaking. In the present work, adaptive mesh refinement (AMR) is utilized to give high-fidelity simulations of the plunging jet and air entrainment associated with the breaking bow wave of the KRISO Container ship (KCS) model at Fr=0.35. To provide the high spatial resolution needed for the solution features, the bow region grid of interest is dynamically deformed and relocated during the simulation. The free surface is captured using the Multicut Piecewise-linear Interface Calculation (MPLIC) method. Dynamic load balancing (DLB) is also used in this study to improve the effective use of computer resources. The velocity components and the characteristic of the vorticity around breaking region predicted by CFD are compared with the experimental data. The results show that the present high-fidelity modeling by AMR-DLB approach can give relatively good predictions of the nonlinear phenomena in bow wave breaking.

KEY WORDS: high-fidelity simulation, bow wave breaking, adaptive mesh refinement, dynamic load balancing

INTRODUCTION

The waves will roll over at the high-pressure area at the bow of ship at high speed due to the blocking action of the bow. Bow wave breaking results in energy loss, which forms breaking wave resistance and lower the propulsion efficiency of the ship. At the same time, large-scale bubble wake phenomenon will be formed behind the ship for a long time, which will affect the stealth of military ships. As a consequence, many academics have long focused on bow breaking, and a lot of research has been done in this area.

At present, there are two main methods to study bow breaking phenomenon: ship model test and numerical simulation. Baba(1969) first observed through experiments that bow wave breaking would lead to a significant increase in the total resistance of the ship. He suggests that the new drag component still satisfies Froude's law of similarity and that the component can be derived from the measured head losses occurring near the free surface and outside the usual frictional wake zone.Olivieri et al. (2003) measured bow and shoulder waves of standard mode DTMB 2349 at high speed by wave height instrument, and discussed in detail the mean and root mean square values of wave heights in the flow field around the hull.With the application of PIV (particle image velocity) technology in ship model tests, more precise data such as free surface variation, velocity vector field, and vorticity field in the ship's flow field can be obtained.Dong et al. (1997) used PIV technology to study the bow-breaking phenomenon of surface ship DTMB5512 under two working conditions of Fr=0.28 and Fr=0.45 and provided detailed flow fields details such as bow wave height and vorticity. Wang et al. (2020) conducted an experimental study on bow breaking phenomena of KCS ships with different trim and depth posture and discussed the influence of trim and depth on ship breaking respectively.

With the development of high-performance computers in recent years, numerical simulation has become an important method to study the bow-breaking phenomenon. The Reynolds-Averaged Navier-Stokes(RNAS) method is widely used in engineering calculation because of its small calculation amount and accurate calculation precision. Olivieri et al. (2007) used the RANS method to solve the N-S equation and the level-set method to capture the free surface. They numerically simulated the bow-breaking phenomenon of ship DTMB5415 at Fr=0.35 and Fr=0.41. The rolling structure of the bow wave and shoulder wave at Fr=0.35 was analyzed. The rolling gap phenomenon and the obvious scar of the free surface were observed. Wang et al. (2020) carried out model tests and numerical simulations on a standard model KCS ship under 8 operating conditions at Fr=0.26-0.425 where naoe-Foam-SJTU, a self-developed ship hydrodynamics solver based on OpenFOAM, was used for numerical simulation. Combined with the VOF method of interface compression technology, flow field details such as KCS ship wave shape and free surface waveform were obtained. In addition, the 18M grid is used to predict the bow-breaking phenomenon of DTMB 5415 ship type Fr=0.35 in the paper (Wang et al.,2017). By comparing the drag, vorticity field, and velocity fields, the numerical results agree well with the experimental results. It is pointed out that the current VOF-based RANS method can accurately predict the wake region related to fore wave breaking. Wilson used the unsteady RANS method in the software CFD SHIP-IOWA to conduct numerical simulation research on the bow

breaking of a surface ship under different Froude numbers (two high Froude numbers). In the simulation, overset grid technology was used to locally encrypt the bow and stern grids, to better simulate the roll breaking of the hull. The results show that the wave-breaking phenomenon is not obvious at medium speed, but at high speed, the obvious and stable roll-breaking wave will appear around the hull, and the scar between multiple bow wave breaking and roll can be observed.

Bow wave breaking is a high Reynolds number phenomenon, and the turbulent pulsation of bow wave breaking contains a large amount of flow field data, while the RANS method averages the N-S equation, and the flow field pulsation will become smooth. Therefore, some researchers began to try to solve this problem with Detached Eddy Simulation (DES) method. The principle of the DES method is to use the RANS method in the near wall area of the hull to reduce the amount of mesh and ensure the calculation accuracy and use the LES method to solve the flow field in the large-scale flow area away from the wall. Carrica et al. (2010) studied the hydrodynamic characteristics of ship DTMB5512 at a speed of Fr=0.28 based on the DES method. In this paper, 100 million magnitude grids are used, and the results show that the DES method can capture the flow characteristics of the free liquid surface very fine. Wu et al. (2021) used the Delayed Detached Eddy Simulation (DDES) method and the RANS method to study the bow-breaking phenomena of ship DTMB5415 under three conditions of trim by the bow of 1 deg, 0 deg, and -1 deg. the results show that trimming by bow makes the free surface sharper and wave amplitude larger in the breaking bow wave region. It is pointed out that the DDES method can obtain more details of the flow field than the RANS method.

In this paper, we use the solver interFoam in open source software OpenFOAM-v10 to study the bow wave breaking of the KCS model with trim by the bow of 1deg. The organization of this paper is as follows. The mathematical model of the DDES method is firstly introduced. Then the computation conditions of the 6.0702m KCS model is demonstrated. The results are finally discussed and summarized.

NUMERICAL METHOD

The governing equation in this paper can be written as a continuity equation and a momentum equation:

$$\frac{\partial \overline{u_i}}{\partial x_i} = 0 \tag{1}$$

$$\frac{\partial \overline{u_i}}{\partial t} + \frac{\partial \overline{u_j u_i}}{\partial x_j} = -\frac{1}{\rho}\frac{\partial \bar{P}}{\partial x_i} + \frac{\partial}{\partial t}\left[\nu \left(\frac{\partial \overline{u_i}}{\partial x_j} + \frac{\partial \overline{u_j}}{\partial x_i} \right) \right] - \frac{\partial \tau_{ij}}{\partial x_j} \tag{2}$$

Where $\overline{u_i}, \overline{u_j}$ is the average velocity component; x_i, x_j （$i, j = 1,2,3$）is the spatial coordinates of the three directions; ρ is the density of water; P is dynamic pressure; ν is the kinematic viscosity coefficient; τ_{ij} is the sublattice stress tensor and $\tau_{ij} = \frac{2}{3}\delta_{ij}k - 2\nu_t S_{ij}$ according to the Boussinesq vortex viscosity.

After the vorticity viscosity assumption is introduced, the governing equation above also requires turbulence model to remove the vorticity viscosity coefficient ν_t. In this paper, the two-equation $SST\, k-\omega$ model is used to supplement the determination. $SST\, k-\omega$ model was proposed by Menter(2003), which combined the advantages of $k-\varepsilon$ model and $k-\omega$ model. $k-\varepsilon$ model is used to deal with the flow in the boundary layer area near the wall, and $k-\omega$ model is used to deal with the flow in the free shear flow area. In the DDES method proposed in this paper, $SST\, k-\omega$ model can be described as the transport equation of turbulent kinetic energy k and turbulent dissipation rate ω:

$$\frac{\partial k}{\partial t} + \frac{\partial \left(u_j k\right)}{\partial x_j} = \tilde{G} - \frac{k^{3/2}}{l_{DDES}} + \frac{\partial}{\partial x_j}\left[\left(\nu + \alpha_k \nu_t\right) \frac{\partial k}{\partial x_j} \right] \tag{3}$$

$$\frac{\partial \omega}{\partial t} + \frac{\partial \left(u_j \omega\right)}{\partial x_j} = \gamma S^2 - \beta \omega^2 + \frac{\partial}{\partial x_j}\left[\left(\nu + \alpha_\omega \nu_t\right) \frac{\partial \omega}{\partial x_j} \right] + \left(1 - F_1\right) CD_{k\omega} \tag{4}$$

DES model (Spalart et al.,2006) uses the RANS model in the boundary layer and other regions near the wall, and the LES sublattice model in the free shear region far away from the wall. When the grid resolution of a region in the flow field is higher and the mesh size is smaller than the set threshold, the large eddy simulation method will be used to obtain a finer grid in this region. However, near the hull, the characteristic length of turbulence is smaller than that of the local grid, which will activate the RANS method to calculate. Therefore, the DES model is based on the size of the local grid to realize the conversion of the RANS region to the LES region. However, if the LES model is switched too early in the near-wall area, the flow will be separated in advance and the turbulent viscosity will be reduced, thus affecting the calculation of the hydrodynamic performance of the ship. DDES method (Zhao et al.,2016) introduces a delay function based on DES method to optimize characteristic turbulence length and improve calculation accuracy while maintaining the ability of DES to capture vortex structure.

The delay function is:

$$f_{\mathrm{d}} = 1 - \tanh\left[\left(8 r_{\mathrm{d}}\right)^3 \right] \tag{5}$$

r_{d} is the delay factor, and the expression is given as:

$$r_{\mathrm{d}} = \frac{\nu + \nu_{\mathrm{t}}}{\sqrt{u_{ij} u_{ij}}\, k^2 d^2} \tag{6}$$

The characteristic length of DDES turbulence with the introduction of delay factor is:

$$L_{\mathrm{DDES}} = L_{\mathrm{RANS}} - f_{\mathrm{d}} max\left(0, L_{\mathrm{RANS}} - L_{\mathrm{LES}}\right) \tag{7}$$

The Piecewise-linear interface calculation (PLIC) is a geometric reconstruction method for the intersection of gas-liquid interfaces based on the VOF method (Youngs, 1982). After solving the phase fraction transport equation, the PLIC method will add a step of the free surface geometric reconstruction process, which can avoid the folding phenomenon of the free surface when transiting from coarse mesh to fine mesh. The PLIC method divides each grid cell geometrically to match its phase fraction value, that is, approximates the interface with straight line segments within a single cell.However, the PLIC method cannot be applied to mesh cells with multiple interfaces or no resolved interfaces, and the interface interpolation method reverts to the standard interface compression method in OpenFOAM. The MPLIC scheme extends the PLIC scheme to handle multiple surface cuts. In the event that a grid cell requires more than one split, MPLIC executes a topological face-edge-

face walk. If that's still not enough, MPLIC divides the cell into tetrahedrons and applies the cuts to those.The MPLIC method is already integrated with OpenFOAM-v10. The use of MPLIC scheme is just by modifying the divergence scheme in the solver as follow:

div(phi,alpha) Gauss MPLIC;

The Adaptive Mesh Refinement (AMR) is a technology that can dynamically encrypt the grid in the process of computation according to refinement criteria. This technique is widely used in the study of hydrodynamic problems of some simple structures, especially in the case of structured mesh. Wackers(2012) developed directional refinement technology for unstructured mesh in commercial software FINE/Marine and simulated the motion of DTMB5512 under head waves condition. Results indicate that grid refinement is a successful technique for realistic, highly complicated flow calculations in marine hydrodynamics. At present, OpenFOAM-v10 can support octa-tree refinement for hexahedral mesh in 3D examples. As shown in Fig. 1, a hexahedral grid cell is segmented into 8 subgrid cells with 36 faces after an octree refinement. Twelve of the surfaces are located in the parent grid cell, and specific mapping techniques are needed to obtain flow field information.

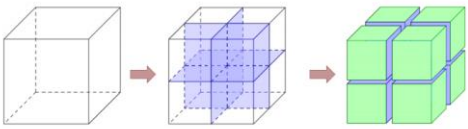

Fig. 1 Octree refinement

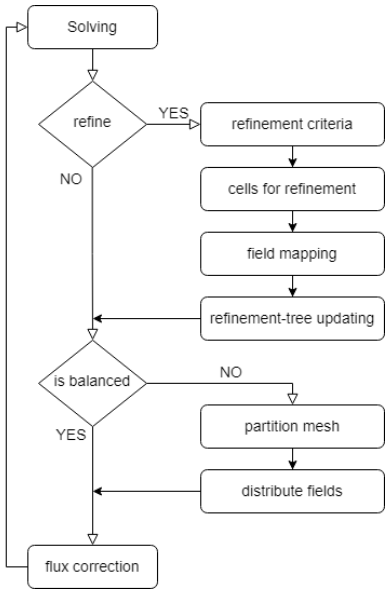

Fig. 2 Flow charts of the mesh refinement

In OpenFOAM, parallel computing is achieved by decomposing the computing domain into different sub-domains, which are allocated to different CPU processors. The most heavily loaded processor becomes the bottleneck when using AMR to handle large-scale parallel transient problems, delaying the progress of all other processors until that processor has finished processing the data. Therefore, for AMR, the Dynamic Load Balancing (DLB) technology can significantly improve the utilization rate of computing resources (Rettenmaier et al.,2019). In simple terms, DLB determines whether to reallocate each processor's computing domain based on the level of load imbalance during the computation. DLB technology has been used in the past to model chemical rapid reaction flows (Tekgul et al., 2021; Morev et al., 2022) whereas this capacity is now included for the first time in the official OpenFOAM-v10 version of the two-phase flow solver interFoam. The mesh refinement process used in this paper by AMR-DLB is shown in Fig. 2.

COMPUTATIONAL CONDITIONS

KCS (KRISO Container Ship) is a modern container ship model designed by KRISO (Korea Research Institute of Ships and Ocean Engineering) in Korea, It is one of the standard ship types often used for CFD verification. In this paper, a 6.0702m KCS model with 1 deg for trim by bow is used for bow breaking wave simulation, and its three-dimensional model is shown in Fig. 3. The main parameters is shown in Table 1. The experiment in this study were conducted in the deep-water towing tank of CSSRC, which is 474 m long, 14 m wide and 7 m deep , with the goal of obtaining the fine flow field of KCS ship breaking waves.

Fig. 3 Geometry of KCS

Table 1. Main parameters of KCS

Parameters	Symbol	Full scale	Present Model
Scale factor	λ	1	37.89
Length between Perpendiculars	L_{PP}(m)	230.0	6.0702
Length on waterline	L_{WL}(m)	224.63	5.9286
Breadth, moulded	B(m)	32.20	0.8498
Draught (F.P.)	T_F	12.80	0.3378
Draught (Midship)	T_M	10.80	0.2850
Draught (A.P.)	T_A	8.80	0.2323
Displacement volume	∇ (m^3)	51130	0.9399

The model test is followed by a numerical simulation to explore bow wave breakup. The gravitational acceleration is set as 9.81 m/s^2, while the velocity is set at 2.7 m/s, corresponding to Fr=0.35. The water's density is set at 998.63 kg/m^3, while the coefficient of kinematic viscosity is set to 1.14×10^{-6} m^2/s. In order to lessen the effect of hull motion on wave breaking, all degrees of freedom are fixed.

Only half of the calculation domain is employed for numerical simulation because this study is focused on the inflow condition of still water, which lowers the cost of calculations. The origin of the axes is located at the point where the waterline and the bow cross in Fig. 4, which also depicts the computational domain and boundary conditions. The incoming flow velocity inlet is set at x=1Lpp length in front of the bow, the pressure outlet is set at x=-3Lpp length after the stern, and the calculation domain is set at 4 times length in the X-axis direction. The bottom boundary, right boundary, and ship's center line plane are all designated as symmetric boundary conditions. The bottom boundary is set at z=-1Lpp, while the right boundary is 1.5Lpp from the ship's midline plane. The upper portion is set at z=0.5Lpp on the free surface with atmospheric boundary conditions.

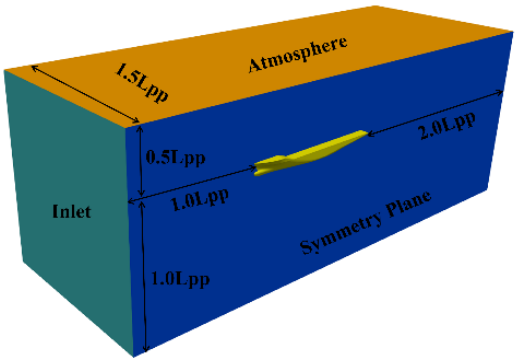

Fig. 4 Computation domain

In this simulation, the snappyHexMesh tool is employed to generate full hexahedral unstructured mesh, and the total mesh amount is 2.2 million. In three directions, there are 80×24×36 initial grids. As shown in Fig. 5, to accurately capture the interface, the free surface is refined to 1/16 of the background grid. Two refinement boxes are set up, one refined to 1/8 of the background grid and the other refined to 1/16, to predict the waves around the hull and small-scale characters. In addition, it should be pointed out that the bow-breaking phenomenon of the KCS model is previously studied using a large number of grids(Wu et al.,2021; Wang et al.,2020; Yu et al.,2019), but in this research, we focus more on the wave-breaking region and make better use of the AMR calculation by omitting the boundary layer from the hull.

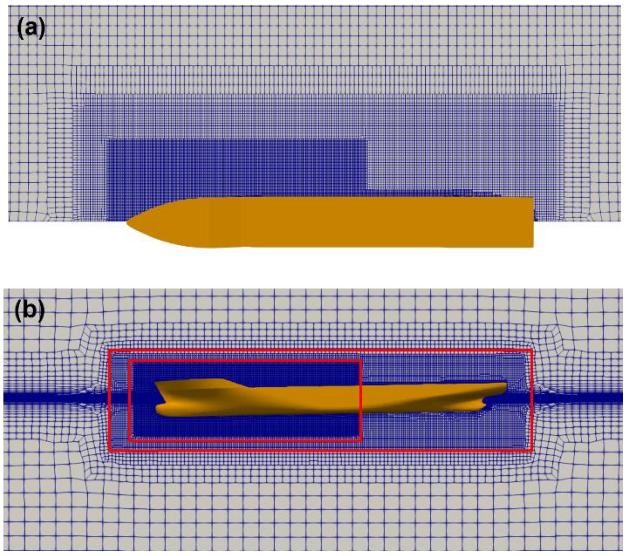

Fig. 5 Mesh distribution and refinement regions set. (a) View 1-Mesh near free surface region; (b) View 2-Mesh from the side view.

RESULTS AND DISCUSSION

In this paper, the bow wave breaking of the KCS ship model at Fr=0.35 is studied. The simulation of the free surface and the complex wave pattern formed by the bow, consisting of sharp breaking waves and many weak secondary waves, is of particular interest in this case. Therefore, a high-resolution grid in the bow area is required. To save computing resources, the AMR-DLB method is utilized to refine the grid of the wave-rolling area. Two refinement criteria are employed in this case. To begin with, the applicability region of AMR technology is limited to -0.5<X<3.2， 0<Y<1.3， -0.2<Z<0.2, where the bow wave is broken (Wu et al.,2021). The free surface is then refined in the restricted region, resulting in a judgment foundation of 0.1<alpha.water<0.9. Set maxImbance to 0.2, redistributionInterval to 10, and maximum refinement level to 1 for this case. The calculation time step of the case is 0.00005, every 20 time steps are refined, and the end time of the calculation is 20 seconds. The refined grid case costs approximately 230 hours of CPU time with 28 CPU cores. The initial grid case costs approximately 132 hours of CPU time with 28 CPU cores.

The results of adaptive refinement mesh and initial mesh at 20s of the case are obtained in accordance with the settings mentioned above. Fig. 6 shows the refined grid and cross section at X=0.15Lpp. The incoming stream rolls over, creating a gap where it is blocked by the bow and spreading out in the shape of a water hammer, as seen in the right side of the image. The left half of the figure shows the grid structure of this section. The yellow line in the figure represents alpha.water=0.5, which shows that the free surface is refined at the level 1.

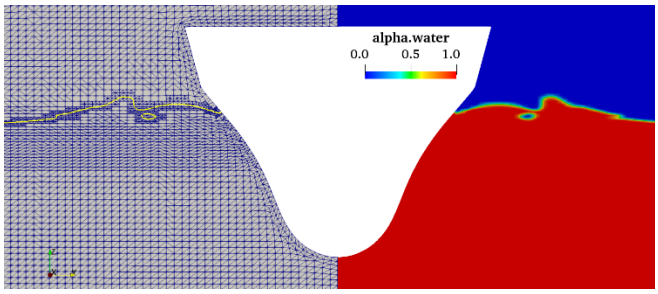

Fig. 6 Cross section at X=0.15Lpp

Fig. 7 shows the comparison of the free surface of the two examples in the 20s. At this point, the refined grid case has 2.4 million grid cells, while the initial grid case has 2.2 million grid cells, representing a grid increment of 8.3%.The above figure is the initial grid result and the following figure is the refined grid result. It can be seen from the figure that the result of the initial grid case is smoother, the outer contour of the bow wave breaking region is rounded, the two main scars are not obvious, and the transition of the scar between each roll is natural. The scar shown by the refined grid case is sharper, and small jets can be observed in the outer contour of the bow wave-breaking region. At the same time, the two cases show that the wave rolls only twice under this working condition, and the wave roll area is constant.. However, it can be found that in the refined grid case, the wave attenuation is more obvious and the ripples caused by fine jets can still be seen, while in the initial grid case, the wave attenuation is less and the flow field details of wave rolling cannot be seen.

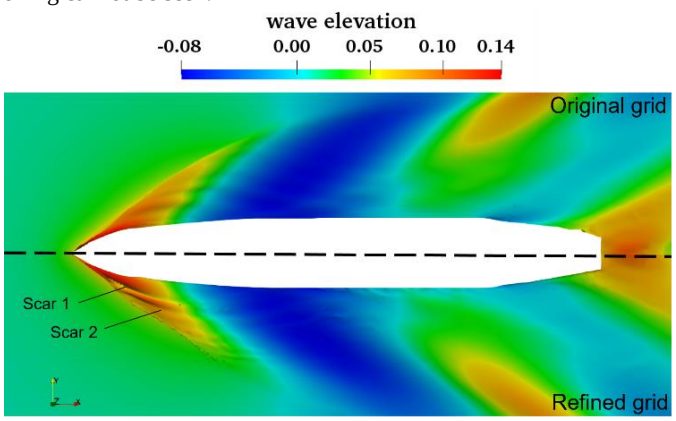

Fig. 7 Comparison of wave contours at Fr = 0.35 (top: Original grid, bottom: Refined grid)

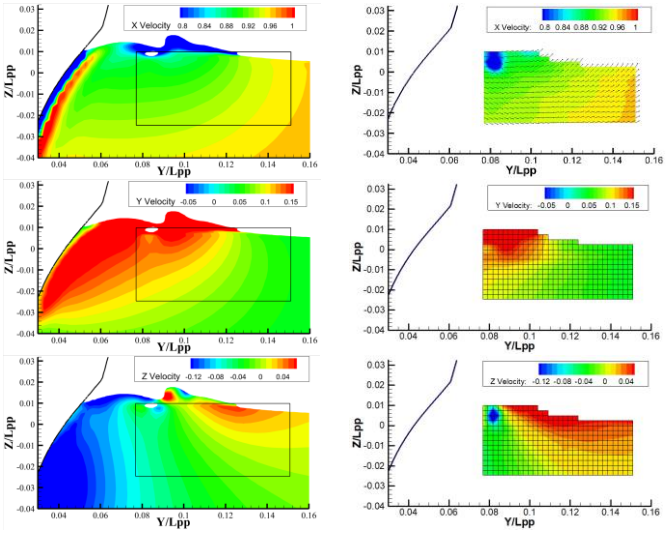

Fig. 8 Comparison of dimensionless velocity distribution at X=0.15Lpp (left: CFD; right:EFD)

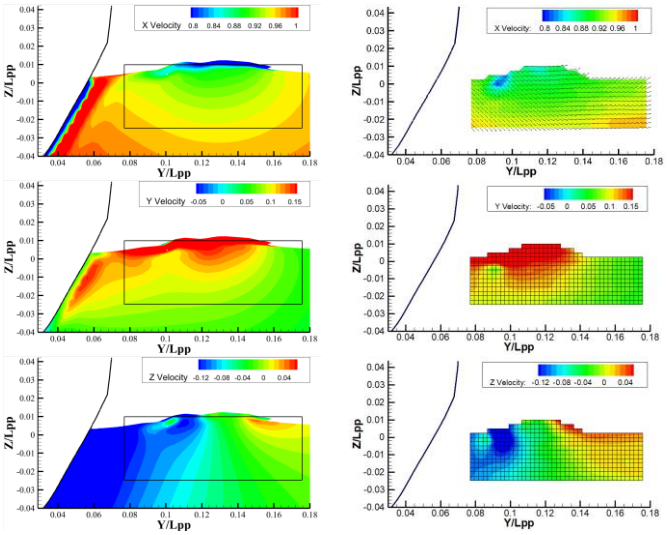

Fig. 9 Comparison of dimensionless velocity distribution at X=0.20Lpp (left: CFD; right:EFD)

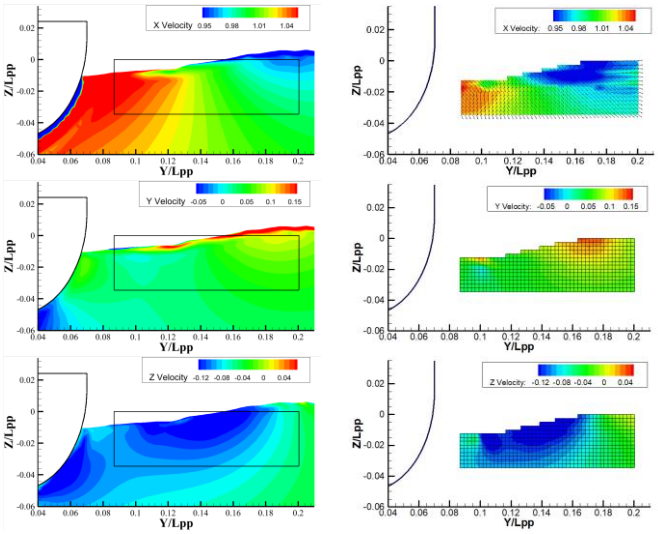

Fig. 10 Comparison of dimensionless velocity distribution at X=0.30Lpp (left: CFD; right:EFD)

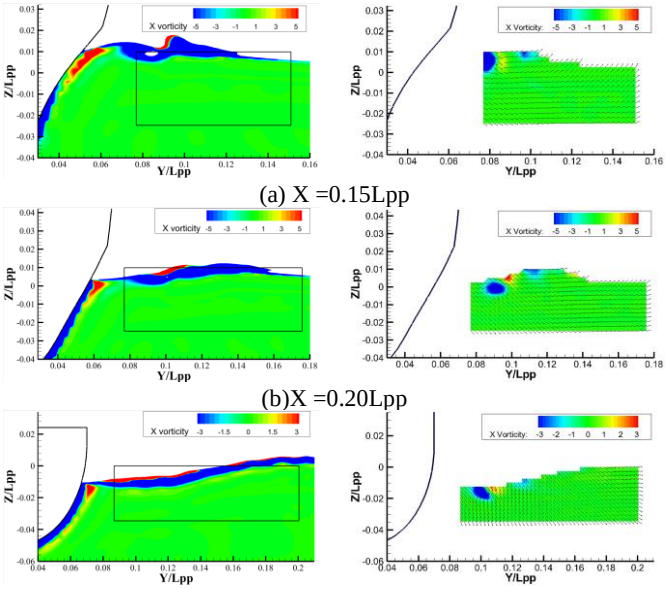

(a) X =0.15Lpp

(b)X =0.20Lpp

(c)X =0.30Lpp

Fig. 11 Comparison of axial vorticity distribution (left: CFD; right:EFD)

Results of XYZ velocity components and X axial vorticity at X=0.15Lpp, X=0.20Lpp, and X=0.30Lpp cross section are given in Figs. 8~11. For each figure, the numerical simulation results are on the left and the experimental results are on the right. With length divided by Lpp = 6.0702m and velocity divided by U=2.7 m/s, all results are dimensionless, corresponding to Fr = 0.35. Positive vorticity indicates counterclockwise rotation, while negative vorticity indicates clockwise rotation.

For cross section X=0.15Lpp, the incoming flow rolls here, generating an air cavity at Y/Lpp=0.08 and a plunging jet at Y/Lpp=0.1. At Y/Lpp=0.08, EFD results forecast an apparent velocity defect zone, whereas CFD results overpredict, but both reveal that a scar occurred at Y/Lpp=0.09. As illustrated in Fig. 11, the air cavity generated by wave curling diffuses the high gradient zone of vorticity to the surrounding area, presenting a negative vorticity value. At the scar point, the longitudinal vorticity presents an obvious positive value, and the positive vorticity region is interwoven with the negative vorticity region.

For cross section X=0.20Lpp, similar to cross section X=0.15Lpp, there is an upward and outward flow trend of the rolling wave. In addition, the velocity defect zone exhibited by CFD and EFD is located at Y/Lpp=0.09, which is further outward than the cross section X=0.15Lpp. It can be clearly found from the vorticity figures that EFD results show two negative vorticity regions at Y/Lpp=0.09 and Y/Lpp=0.11 respectively, while CFD results can contain these two negative vorticity regions, but it is not obvious. Moreover, for both CFD and EFD, it can be found that a scar exists at Y/Lpp=0.1 where positive vortexes and negative vortexes interweave.

For cross section X=0.30Lpp, the free surface changes slightly, but the fluid velocity around the hull also exhibits an outward and upward trend. Due to the influence of the hull shape, the axial velocity near the hull is larger in this section, and the transverse velocity variation gradient is higher. The EFD vorticity figures show that there is an obvious negative vortex zone at Y/Lpp=0.1 and Y/Lpp=0.13, while there is a positive vortex region at Y/Lpp=0.11. In CFD results, the negative vortex region

presents strip distribution, and there is a strip discontinuous positive vortex region near the free surface. This means that in this section, the rolling wave is along the free liquid surface, and the amplitude is tiny, so the scars generated are not obvious.

In general, the velocity distribution, vortex structure, and scar distribution predicted by CFD are in good agreement with EFD results. The main difference between EFD and CFD is in the details of vortices. The better capture of bow breaking wave is realized by the refined grid. However, the grid resolution is still insufficient for regions with small changes in the free surface, such as the X=0.30Lpp section, and CFD adopts instantaneous velocity data, which may account for the differences between CFD and EFD results.

CONCLUSIONS

In this paper, we employ AMR-DLB technology to simulate the phenomenon of the bow breaking wave of the KCS model at Fr=0.35. By comparing the wave contours of the initial grid case and the refined grid case, we find refined grid can capture sharper scars and small jets in the bow braking region. Furthermore, the numerical simulation results of XYZ velocity components and X axial vorticity at X =0.15Lpp, X=0.20Lpp, and X =0.30Lpp cross section are discussed on the basis of the experimental data. The result demonstrates that the current high-fidelity modeling by AMR-DLB approach is capable of making reasonably accurate predictions of the nonlinear processes in bow wave breaking.

However, there are still some differences between CFD and EFD results, especially in the velocity defect area near Y=0.1Lpp and the free surface. In the future, we need to use higher refinement level and more accurate refinement criteria to focus on the flow details of bow breaking wave.

ACKNOWLEDGEMENTS

This work was supported by the National Natural Science Foundation of China (52131102), and the National Key Research and Development Program of China (2019YFB1704200), to which the authors are most grateful.

REFERENCES

Baba, E. (1969). "A new component of viscous resistance of ships." *Journal of the Society of Naval Architects of Japan*, 1969(125), 23-34.

Carrica, P. M., Huang, J., Noack, R., et al. (2010). "Large-scale DES computations of the forward speed diffraction and pitch and heave problems for a surface combatant." *Computers & Fluids*, 39(7), 1095-1111.

Dong, R. R., Katz, J., Huang, T. T. (1997). "On the structure of bow waves on a ship model." *Journal of Fluid Mechanics*, 346, 77-115.

Menter, F. R., Kuntz, M., Langtry, R. (2003). "Ten years of industrial experience with the SST turbulence model." *Turbulence, heat and mass transfer*, 4(1), 625-632.

Morev, I., Tekgül, B., Gadalla, M., et al. (2022). "Fast reactive flow simulations using analytical Jacobian and dynamic load balancing in OpenFOAM." *Physics of Fluids*, 34(2), 021801.

Olivieri, A., Pistani, F., Mascio, A. D. (2003). "Breaking wave at the bow of a fast displacement ship model." *Journal of marine science and technology*, 8(2), 68-75.

Olivieri, A., Pistani, F., Wilson, R., et al. (2007). "Scars and Vortices Induced by Ship Bow and Shoulder Wave Breaking." ASME. *J. Fluids Eng*. November 2007; 129(11): 1445–1459.

Rettenmaier, D., Deising, D., Ouedraogo, Y., et al. (2019). "Load balanced 2D and 3D adaptive mesh refinement in OpenFOAM." *SoftwareX*, 10, 100317.

Spalart, P. R., Deck, S., Shur, M. L., et al. (2006). "A new version of detached-eddy simulation, resistant to ambiguous grid densities." *Theoretical and computational fluid dynamics*, 20(3), 181-195.

Tekgül, B., Peltonen, P., Kahila, H., et al. (2021). "DLBFoam: An open-source dynamic load balancing model for fast reacting flow simulations in OpenFOAM." *Computer Physics Communications*, 267, 108073.

Wackers, J., Deng, G., Leroyer, A., et al. (2012). "Adaptive grid refinement for hydrodynamic flows." *Computers & Fluids*, 55, 85-100.

Wang, J., Wan, D. C. (2017). "Breaking wave simulations of high-speed surface combatant using OpenFOAM." In *Proceedings of the 8th International Conference on Computational Methods (ICCM2017)* (pp. 25-29).

Wang, W., Qiu, G., Wang, J., Wan, D. (2020). "Experimental and Computational Investigations on KCS Wave Breaking with Trim and Sinkage Variation." In *The Fourteenth ISOPE Pacific/Asia Offshore Mechanics Symposium*. OnePetro.

Wei-wen, Z. H. A. O., De-cheng, W. A. N. (2016). "Detached-Eddy Simulation of Flow Past Tandem Cylinders." *Applied Mathematics & Mechanics* (1000-0887), 37(12).

Wu, D., Wang, J., Wan, D. (2021). "Delayed detached eddy simulation method for breaking bow waves of a surface combatant model with different trim angle." *Ocean Engineering*, 242, 110177.

Youngs, D. L. (1982). "Time-dependent multi-material flow with large fluid distortion." *Numerical methods for fluid dynamics*.

Yu, A., Wan, D. (2019). "RANS model for bow wave breaking of a KRISO Container Ship under different speeds." In *11th International Workshop on Ship and Marine Hydrodynamics (IWSH2019)*.